High-Speed AFM and Applications to Biomolecular Systems

Toshio Ando,[1,2] Takayuki Uchihashi,[1,2] and Noriyuki Kodera[2]

[1]Department of Physics and [2]Bio-AFM Frontier Research Center, Kanazawa University, Kanazawa 920-1192, Japan; email: tando@staff.kanazawa-u.ac.jp

Keywords

Abstract

Directly observing individual protein molecules in action at high spatiotemporal resolution has long been a holy grail for biological science. This is because we long have had to infer how proteins function from the static snapshots of their structures and dynamic behavior of optical makers attached to the molecules. This limitation has recently been removed to a large extent by the materialization of high-speed atomic force microscopy (HS-AFM). HS-AFM allows us to directly visualize the structure dynamics and dynamic processes of biological molecules in physiological solutions, at subsecond to sub-100-ms temporal resolution, without disturbing their function. In fact, dynamically acting molecules such as myosin V walking on an actin filament and bacteriorhodopsin in response to light are successfully visualized. In this review, we first describe theoretical considerations for the highest possible imaging rate of this new microscope, and then highlight recent imaging studies. Finally, the current limitation and future challenges to explore are described.

Contents

INTRODUCTION

Atomic force microscopy (AFM) was originally invented to visualize atoms on solid surfaces (10). In biological sciences, this microscopy is now routinely used to directly acquire high-resolution images of biological samples under physiological conditions, without sample staining (66, 81, 82). AFM is also used for the recognition and localization of specific molecules (37, 91) as well as force measurements to estimate the strength of intra- and intermolecular bonds at the single-molecule level (26, 67, 108), the elasticity of biological surfaces (19, 98), and the osmotic pressure of live cells (90). Therefore, AFM is a nano-toolbox for biology (reviewed in References 64 and 65). However, the limited scan speed of AFM limits its usefulness. It takes time (at least 30 s) to acquire an image, and therefore, molecules moving on the substrate surface are imaged as a blur or cannot be imaged at all. To overcome this limitation, the development of high-speed AFM (HS-AFM) was started around 1993. Through the initial prototypes (5, 103, 104) and their extensive improvements (8, 9, 24, 25, 29, 47, 50, 51, 53, 101), HS-AFM is now materialized (3, 7). Although the speed performance depends on imaging conditions, current HS-AFM can generally capture an image of biological molecules within 100 ms or less. Importantly, the structure and function of fragile molecules are not disturbed by the interaction with a cantilever tip. This high-speed and low-invasive performance opens up a new opportunity to visualize dynamically functioning biological molecules in great detail. As has been demonstrated in recent imaging studies (12, 40, 52, 86, 99), the visualized dynamic images of proteins can provide information inaccessible with other approaches, giving great insight into how the proteins function. Remarkably, the dynamic images can be interpreted straightforwardly without intricate analyses and interpretations, making it possible to attain firm conclusions. This review summarizes the fundamentals of HS-AFM, highlights recent imaging studies of proteins, and outlines ongoing and future challenges to expand the scope of its application to biological studies.
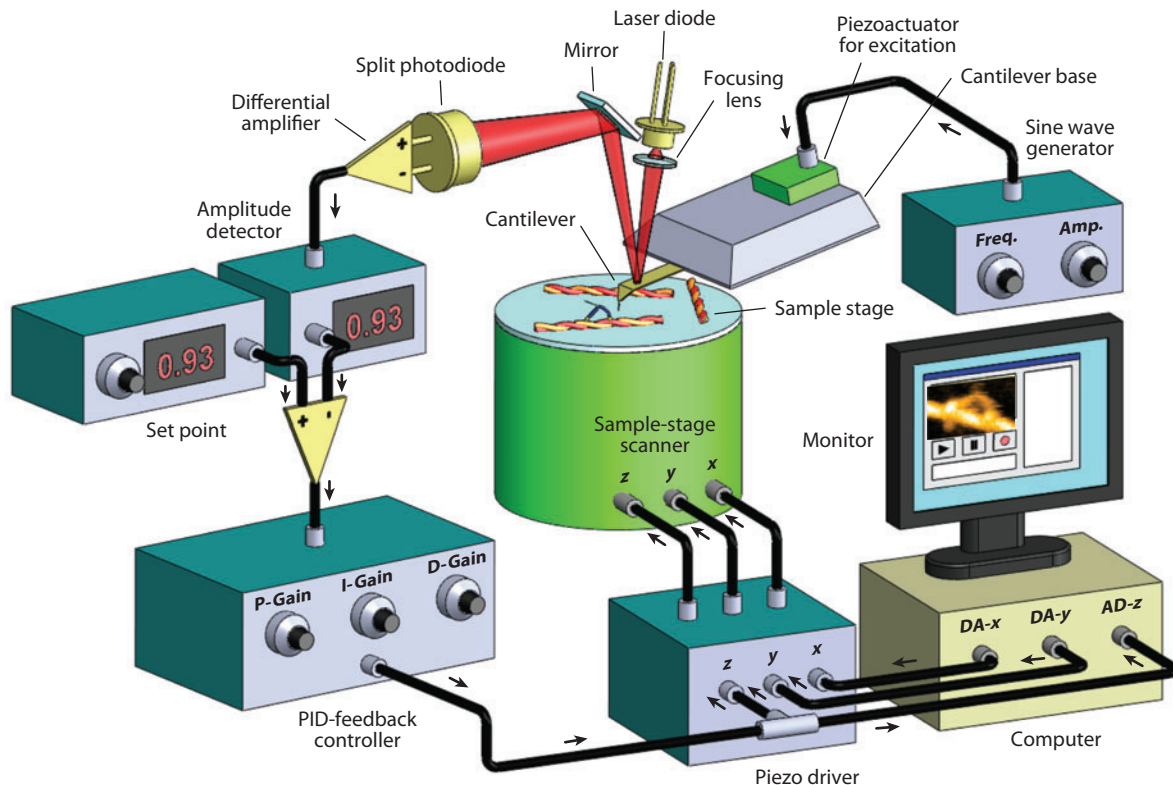
AFM: atomic force microscopy

Figure 1

Schematic for general configuration of a tapping-mode AFM system (see text for details).

FEEDBACK OPERATION AND MAXIMUM POSSIBLE IMAGING RATE

Visualization by AFM of the topography of a sample placed on a substrate surface requires acquisition of sample height information over many points on the sample surface (**Figure 1**; **Supplemental Movie 1**, follow the **Supplemental Material link** from the Annual Reviews home page at **http://www.annualreviews.org**). A stylus probe attached to the free end of a cantilever is brought into contact with the sample. Mechanical response of the cantilever upon this contact is measured and then the sample stage is finally moved in the z-direction to recover the mechanical state of the cantilever back to a given condition (i.e., set point) through feedback control. For this recovery, the closed feedback loop spends a certain amount of time mainly because of the slow response of the mechanical devices (i.e., cantilever and z-scanner). This series of operations is repeated many times for different sample surface points during lateral scanning of the sample stage. Among several imaging modes of AFM (reviewed in References 31 and 63), the tapping mode (120) (also called amplitude modulation mode or intermittent contact mode) is often used for biological samples. In this mode, the cantilever is oscillated in the z-direction at its first resonant frequency (**Supplemental Movie 1**) so that the tip intermittently taps the sample surface. This tapping results in decreased amplitude as well as a phase shift relative to the excitation signal (101). The intermittent contact can eliminate friction force during lateral scanning, which minimizes deformation of fragile biological samples. Described below

Supplemental Material

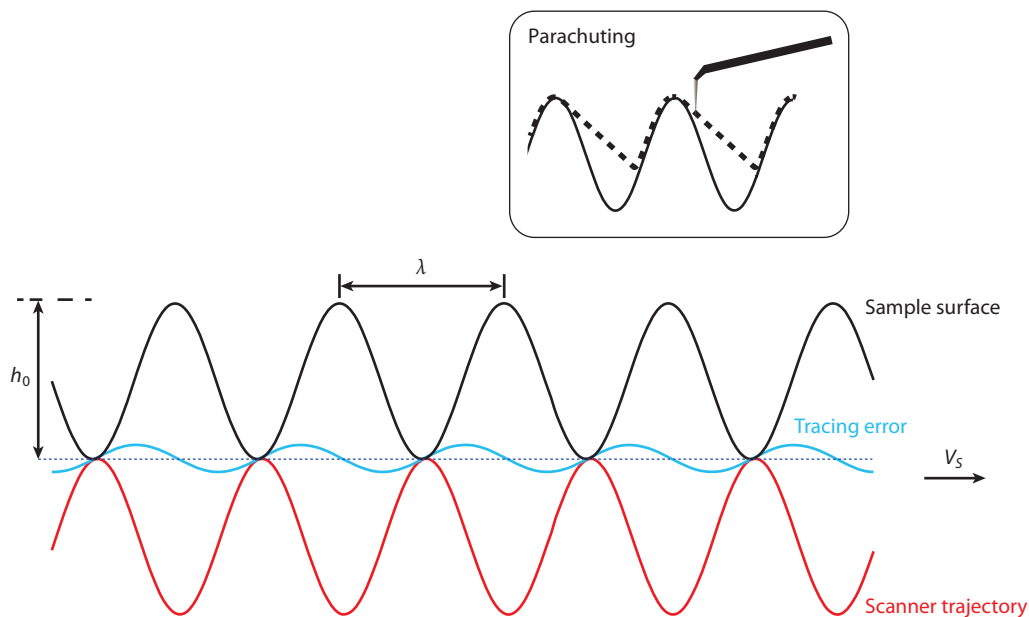**Set point:** the target value of a controlled variable

Figure 2

Scanner movement tracing sinusoidally shaped sample surface with periodicity λ and amplitude $h_0/2$, when no parachuting occurs. The inset shows a trajectory of the bottom swing position of the tip (*broken line*) relative to the sample surface when parachuting occurs.

is the feedback operation to maintain the cantilever oscillation amplitude (and thus tip-sample interaction force) constant. Next, the highest possible imaging rate of tapping-mode HS-AFM is derived as a function of the feedback bandwidth and various parameters.

Feedback Operation

In the closed feedback loop (see **Figure 1**), the input to the loop is the variation of sample height right under the cantilever tip and the output is the displacement of the z-scanner. The output from the feedback controller is used as a signal representing the sample height. There are several devices in the feedback loop: a cantilever, an optical beam deflection (OBD) detector for the detection of cantilever deflection, an amplitude detector (deflection-to-amplitude converter), a feedback controller, a piezoelectric driver, and a piezoactuator-based z-scanner. Each of these devices has a certain time delay in the response to the corresponding input signal. Therefore, the feedback control cannot perform without time delay. This delay deteriorates the speed performance of the microscope, which is described below.

For simplicity, it is assumed that the sample surface profile in the x-z plane has a sinusoidal shape with a periodicity λ and an amplitude $h_0/2$ (**Figure 2**, black line). When the sample-stage scanner is moved in the x-direction at velocity V_s, the sample height h right under the cantilever tip changes with time as

OBD: optical beam deflection

$$h(t) = (h_0/2) \times \sin(2\pi f t), \qquad \qquad 1.$$

where $f = V_s/\lambda$. During feedback scan, the z-scanner moves in the direction opposite to the sample height so that the sample surface looks flat when viewed from the cantilever. However, because

of the time delay (τ_0) in the closed feedback loop, the z-scanner moves at feedback frequency f as

$$z(t) = -(h_0/2) \times \sin(2\pi f t - \theta), \qquad 2.$$

where $\theta = 2\pi f \tau_0$ (**Figure 2**, red line). Therefore, the sample surface when viewed from the cantilever does not look perfectly flat but varies with time as

$$S(t) = h(t) + z(t) = h_0 \sin(\theta/2) \cos(2\pi f t - \theta/2). \qquad 3.$$

The deviation from a flat surface (i.e., feedback error) due to the feedback delay is indicated with the blue line in **Figure 2**. When cantilever free oscillation amplitude and the amplitude set point are set at A_0 and A_s ($= rA_0$; $0 < r < 1$), respectively, the cantilever tip in contact with the sample surface is pushed upward by the sample to an extent of $D(t) \equiv S(t) + A_0(1 - r)$ so long as the sample is rigid enough compared with the cantilever.

The feedback bandwidth f_B, which is a value characterizing the speed performance of feedback operation in the AFM system, is usually defined by a feedback frequency at which 45° phase delay occurs in the feedback scan. Thus, $f_B = 1/(8\tau_0)$. Because the feedback frequency f should not exceed f_B, a condition $f < f_B$ holds, which limits the scan speed V_s as $V_s < \lambda f_B$.

Other Factors Limiting Feedback Frequency

However, two other factors limit f more severely than f_B. One comes from the condition that $D(t)$ should always be positive. Otherwise, at downhill regions of the sample, the cantilever tip cannot make contact with the sample surface at the bottom swing of oscillation; i.e., parachuting occurs (**Figure 2**, inset). Once detached, the error signal is saturated at $A_0(1 - r)$. When r is set close to 1 so that the tapping force exerted from the oscillating cantilever tip to the sample is minimized, the saturated error signal is small, and hence the parachuting time is prolonged (51, 92). During parachuting, the sample topography cannot be recorded at all. The condition under which no parachuting occurs is expressed as

$$A_0(1 - r) - h_0 \sin(\theta/2) > 0. \qquad 4.$$

To minimize the tapping force, small A_0 has to be used in addition to r close to 1. For example, for $A_0 = h_0/5$ and $r = 0.9$, Equation 4 limits the phase delay as $\theta < 2.3°$, which severely limits the feedback frequency f as $f < 0.05 f_B$. The other condition that limits f comes from the maximum possible tapping force under which the structure and function of the biological sample are retained. The maximum tapping force F_p^{max} is exerted at an uphill region of the sample, which can be approximately expressed as

$$F_p^{max} = (k_c/Q_c) \times [A_0(1 - r) + h_0 \sin(\theta/2)], \qquad 5.$$

where k_c and Q_c are the spring constant and the quality factor in water of the cantilever, respectively. For example, under the condition of $F_p^{max} = 100$ pN, $k_c = 200$ pN/nm, $Q_c = 2$, $A_0 = 1$ nm, $h_0 = 5$ nm, and $r = 0.9$ [these values are realistic ones as values close to these values are actually used in successful imaging of functioning proteins (40, 52, 86, 99)], Equation 5 limits the phase delay as $\theta < 20.7°$, which moderately limits f as $f < 0.46 f_B$.

Thus, the parachuting problem is the severest limiting factor for the maximum possible feedback frequency and hence for the scan speed V_s. However, we have successfully eliminated this problem by developing a feedback controller that can automatically change its gain parameters depending on the cantilever oscillation amplitude during imaging; feedback gain is increased at the downhill region of the sample so that parachuting only rarely occurs (51). Even when it occurs, the parachuting time is reduced significantly.

Here, note that the mechanical quantity affecting the sample (i.e., causing momentum change) is not the tip force itself acting on the sample but the impulsive force (the product of the force acting on the sample and the time for which the force acts). When the cantilever resonant frequency is high (~1 MHz in water), as is the case for small cantilevers optimized for HS-AFM, the force acting time is approximately 100 ns or less, which guarantees no significant effect of $F_p^{max} = 100$ pN on fragile protein molecules.

Maximum Possible Imaging Rate

The maximum possible imaging rate R_{max} is a function of f_B and the imaging condition (the scan size in the x-direction W, the number of scan lines N, and the spatial frequency of sample height corrugation to be imaged $1/\lambda$) as well as of the maximum possible phase delay θ_{max} in the feedback operation that depends largely on the sample fragility. For given W, N, and V_s, one frame of image is captured with time $T = (2WN)/V_s$. The maximum possible scan speed V_s^{max} is given by $\theta_{max}/(\pi/4) \times \lambda f_B$. Thus, R_{max} is given by

$$R_{max} = 2\theta_{max}\lambda f_B/(\pi W N). \qquad 6.$$

For example, under a realistic condition for imaging protein molecules by our HS-AFM ($f_B = 110$ kHz, $\theta_{max} = \pi/9$ (i.e., 20°), $\lambda = 10$ nm, $W = 150$ nm, and $N = 100$), Equation 6 gives $R_{max} = 16.3$ frames per second (fps). The high f_B achieved (110 kHz) is approximately 1,000 times higher than that of conventional AFM systems.

CANTILEVER, SAMPLE STAGE, AND SUBSTRATE SURFACE

HS-AFM is materialized by the achievement of three conditions to meet high-speed and low-invasive performance: (*a*) extensive reduction of time delays in the response of all devices contained in the feedback loop (reviewed in Reference 7), (*b*) damping of mechanical vibrations caused by fast displacement of the scanner (7, 53), and (*c*) feedback control technique that can eliminate tip parachuting even when A_s is set close to A_0 (51). Details of various techniques and devices that have achieved these conditions are described elsewhere (7). The latest HS-AFM instrument developed by us is commercially available from the Research Institute of Biomolecule Metrology Co., Ltd. (Tsukuba, Japan). Here, we therefore focus on devices (small cantilevers, sample stage, and substrate surfaces) and associated issues that HS-AFM users themselves must deal with.

Small Cantilevers

When a cantilever tip taps the sample surface, a brief stepwise force is exerted on the cantilever. The cantilever responds to this force with a response time $\tau_c = Q_c/\pi f_c$, where f_c is the first resonant frequency of the cantilever in water. Measuring the cantilever oscillation amplitude requires time, at least $\tau_m = 1/2f_c$. Thus, the resonant frequency f_c should be as high as possible, whereas k_c should be small for fragile biological samples. Q_c can be naturally small in water. The size of the cantilever has to be small to achieve both high f_c and small k_c (50, 104). Several types of small rectangular cantilevers made of Si_3N_4 have been developed by Olympus (Tokyo, Japan) in collaboration with our group. The high-end small cantilevers (Olympus BL-AC7DS-KU5, custom-made) that we have been routinely using for imaging studies are 6–7 μm long, 2 μm wide, and 90 nm thick (**Figure 3*a***). They have $f_c = 1.2$ MHz in water (3.5 MHz in air), $Q_c \approx 2$ in water, and $k_c = 0.2$ N/m. The commercially available small cantilevers (Olympus BL-AC10DS-A2) are 9–10 μm long, 2 μm wide, and 130 nm thick, and have $f_c = 0.6$ MHz in water (1.5 MHz in
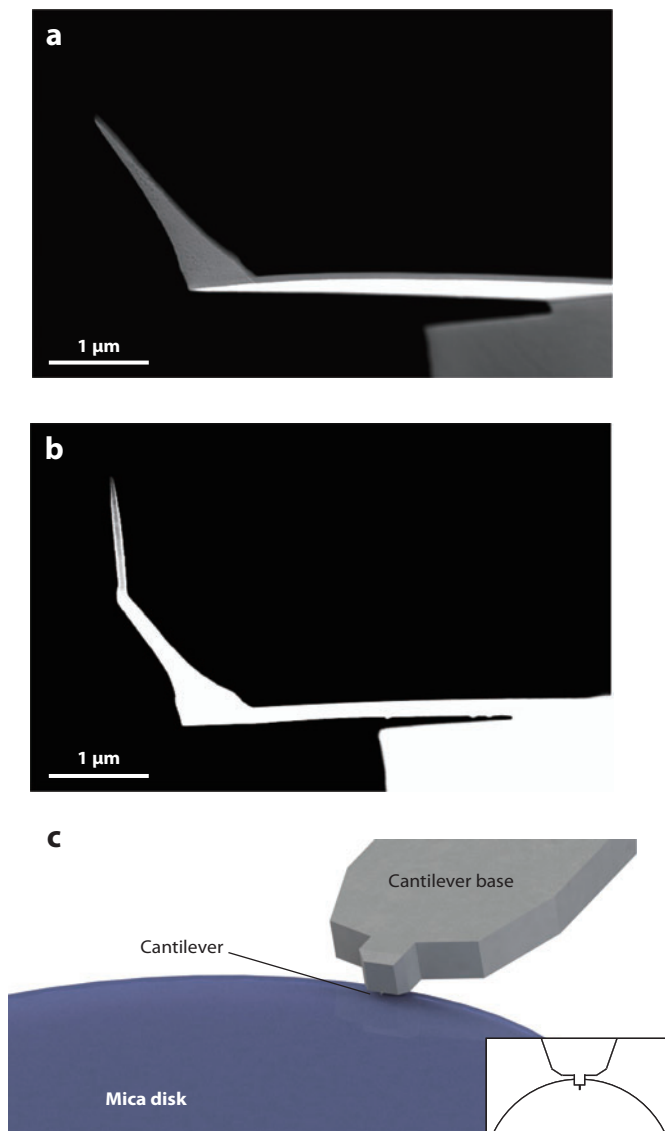
Figure 3

Cantilever, tip, and relative arrangement of cantilever and sample stage. (*a*) Scanning electron microscope (SEM) image of a small cantilever. (*b*) SEM image of an electron-beam-deposited (EBD) tip grown on an original bird-beak-shaped tip. (*c*) Relative arrangement between sample stage and cantilever for circumventing the disturbance by hydrodynamic pressure produced by quick displacement of the *z*-scanner.

air), $Q_c \approx 2$ in water, and $k_c = 0.1$ N/m. Small cantilevers are also available from NanoWorld (Neuchâtel, Switzerland).

Small cantilevers have other advantages. The total thermal noise $(k_B T/k_c)^{1/2}$ (where k_B is Boltzmann's constant and T is the temperature in Kelvin) (2) is distributed over frequencies up to slightly above f_c. Therefore, a cantilever with a higher f_c has a lower noise density. In the tapping

mode, the frequency region used for imaging is approximately the feedback frequency centered on the resonant frequency. Thus, for a cantilever with a higher f_c, thermal noise has less effect on the amplitude measurement. The deflection of a cantilever alters the angle of its free end ($\Delta\varphi$), which is detected by the OBD detector (see **Figure 1**). Therefore, for a given displacement Δz of the cantilever free end in the z-direction, a shorter cantilever results in a larger angle change ($\Delta\varphi = 3\Delta z/2L$) and thus gives higher displacement detection sensitivity. Because of a small thermal noise effect and this high sensitivity with small cantilevers 6–10 μm long, the displacement as small as <0.1 nm can be detected even with high bandwidth detection (a few megahertz). The deflection-to-amplitude conversion can be performed every half or one cycle of cantilever oscillation using fast amplitude detectors developed (5, 7).

The bird-beak-shaped tip of the small cantilevers produced by Olympus is approximately 1.5 μm long and its apex radius is 15–24 nm. Small cantilevers that have an additional carbon nanofiber tip with an apex radius <10 nm grown on the bird-beak-shaped tip have become commercially available (Olympus, BL-AC10FS-A2) (49, 97). When a scanning electron microscope (SEM) is available, electron-beam-deposited (EBD) tips can be grown under an atmosphere of gas sublimated from materials. Various materials can be used for the deposition of carbon, platinum, tungsten, and silicon dioxide. A gas injection system, which is adaptable to SEMs and can mix different gases under computer control, is commercially available (Omniprobe OmniGIS™). The grown tips can be sharpened by nitrogen or oxygen plasma etching. The tip apex radium is usually reduced to ~5 nm and sometimes to ~0.5 nm (100).

Sample Stage and Hydrodynamic Pressure

In high-speed imaging, the sample-stage z-scanner is displaced at high frequencies (20–100 kHz). This fast scan exerts a hydrodynamic pressure on the cantilever and its supporting base placed in close vicinity to the sample surface, which tends to move them, particularly when the sample stage is large (4). Their movement results in a slow response of the cantilever oscillation amplitude to z-scanner displacement. In the worst case, this delay extends to a few microseconds (6, 100), which is much longer than the minimized time delay in the closed feedback loop. As a sample stage, a small glass rod 1.5–2 mm in diameter and 2 mm high is routinely used for HS-AFM imaging (**Figure 3c**).

To further circumvent the disturbance by hydrodynamic pressure, the cantilever is positioned in a way that the whole cantilever chip minimally overlaps with the sample stage when viewed from the top (**Figure 3c**). Moreover, the cantilever tip longer than ~2.5 μm is prepared by the growth of a >1-μm-long EBD tip on the original tip (**Figure 3b**). When the tip is shorter, the cantilever gets closer to the sample surface at the bottom of swing and thus the solution confined between them becomes more squeezed, resulting in oscillation damping and the deteriorated detection sensitivity of tip-sample interaction (6).

Substrate Surfaces

A substrate surface, on which a sample is placed, holds the key to successful HS-AFM imaging (reviewed in References 109 and 111). The surface should be flat enough so that the molecules of interest deposited on it can be easily identified. Observing dynamically acting protein molecules requires the substrate surface to loosely bind the molecules to allow them to retain their physiological function. However, the sample-surface interaction is essential to avoid too rapid Brownian motion of the sample, particularly for single-protein molecules isolated completely from other molecules. Observing dynamic interactions between different proteins often requires selective protein attachment to a surface. As substrate surfaces, bare or chemically treated mica surfaces,

planar lipid bilayer (PLB) surfaces, and the surfaces of two-dimensional crystals of streptavidin formed on a biotin-containing PLB have been used for dynamic AFM imaging. The properties of these surfaces are summarized below.

Mica surfaces. Mica (natural muscovite or synthetic fluorophlogopite) has been frequently used as the substrate source because of its surface flatness at the atomic level over a large area. It has a net negative charge and is therefore quite hydrophilic. A bare mica surface adsorbs DNA and various proteins by electrostatic interaction. We can control the adsorption strength by varying the ionic strength or pH or by adding divalent cations such as Mg^{2+} and Ni^{2+} (especially for attaching negatively charged samples) (17, 72). Monovalent cations markedly change the affinity; $Li^+ > Na^+ > K^+$ for every protein (18). For fractionated membranes containing membrane proteins, the bare mica surface is useful. A water layer of ~1 nm thickness separates the membranes from the mica surface, enabling the motion of membrane proteins within the membranes (46, 76, 113). Proteins, including proteins in membranes, can be covalently immobilized onto chemically treated mica surfaces (43).

Planar lipid bilayer surfaces. PLB can easily be formed on a bare mica surface by the deposition of liposomes (58). The PLB surfaces can be used for both specific and electrostatic immobilizations of proteins. For the specific immobilization of biotinylated proteins and His-tag-conjugated proteins, lipids with biotin and nickel–nitrilotriacetic acid (Ni–NTA) at the polar head groups can be used, respectively. Multiple-point pinning is sometimes required for stopping the rapid motion of molecules tethered to the surfaces. PLB surfaces prepared with electrically neutral phospholipids are resistant to the nonspecific binding of proteins. For electrostatic immobilization, lipids with charged head groups can be used. Unlike bare mica surfaces, the surface charge density and polarity can be varied by using different fractions of a charged lipid and by using positively or negatively charged lipids, respectively.

Streptavidin two-dimensional crystal surfaces. The two-dimensional crystals of streptavidin can easily be formed on highly fluidic PLBs containing lipids with unsaturated alkyl chains (such as DOPC, dioleoylphosphatidylcholine) and a biotin-containing lipid (11, 20). Their surface is particularly useful for the selective and stable immobilization of homo-oligomeric protein complexes because pinning the complexes at multiple biotinylated sites is possible (109). Not only biotinylated samples but also His-tag-conjugated samples can be immobilized using biotin-Ni-NTA compounds as a linker. Importantly, the surface is resistant to the nonspecific binding of proteins.

IMAGING OF PROTEINS IN ACTION

The imaging studies conducted thus far have covered a wide range of dynamic molecular events (reviewed in References 3, 14, and 44). These events are classified into (*a*) structure dynamics of proteins including myosin V on actin (52), rotorless F_1-ATPase (99), P2X$_4$ receptors (87), bacteriorhodopsin (bR) (85, 86), Ca^{2+} pump (118), and intrinsically disordered FACT protein (61); (*b*) self-assembly processes including amyloid-like fibril formation from cleaved lithostathine (57) and PLB formation (3, 33); (*c*) dynamic protein-protein interactions including GroEL-GroES (8, 109, 119), membrane-mediated association between c-rings of ATP synthase (15), bR trimer-trimer (13, 113), and DNA-histone (60, 94); (*d*) diffusion processes including OmpF reconstructed in lipids at high density (12), porin trimers on a live bacterial cell surface (112), defects in protein two-dimensional crystals (110), and DNA-bound Rad54 (79); (*e*) molecular processes associated with enzymatic reactions including cellulase hydrolyzing cellulose fibers (39, 40) and DNA restriction-modification enzymes (32, 93); and (*f*) dynamics occurring with DNA

origamis (22, 23, 80, 96, 107). Below we give two examples of imaging studies of proteins in action to demonstrate the power of HS-AFM.

Myosin V Walking on Actin Filament

Double-headed myosin V (M5) functions as a cargo transporter in cells (reviewed in 83) and moves processively along an actin filament toward the plus end of the filament (56, 77) in a hand-overhand manner with a 36-nm advance (28, 106, 116) for every ATP hydrolysis cycle (78). Hand-overhand means that the two heads step alternately, exchanging leading and trailing roles at each step, very much like walking. We visualized the walking molecules by HS-AFM (52). Below, we describe an experimental setup for this visualization and what we can learn by closely looking at walking molecules.

Selection of substrate surface. Partially biotinylated actin filaments were immobilized on the surface of PLB containing an electrically neutral phospholipid, a biotin lipid, and a positively charged lipid, through streptavidin with a low surface density. When the positively charged lipid was absent, tail-truncated M5 (M5-HMM) was never bound to the surface and only interacted with the immobilized actin filaments to move unidirectionally. The velocity of the movement was identical to that measured by fluorescence microscopy under the same buffer solution. However, most of the molecules were moving, orienting perpendicularly to the surface, so that their structure was not well resolved (**Figure 4a**). When a positively charged lipid was included in the bilayer at an appropriate density, we could observe the characteristic sideways topography of the molecules processively moving with ∼36-nm steps at slightly lower velocity (**Figure 4b**; **Supplemental Movie 2**). However, we could not see detailed molecular behavior during a step because it was completed within a frame time (1/7 s). To slow down the step, streptavidin molecules were further placed on the substrate surface as moderate obstacles to the advance. This method allowed the visualization of stepping processes as shown in **Figure 4c,d** (see also **Supplemental Movie 3**).

Supplemental Material

No effect of tip-sample interaction on motor activity. When streptavidin molecules as moderate obstacles were absent, we could continuously track a moving molecule (up to ∼20 steps) by shifting the scan area manually, while observing the scanned images on a computer display (**Supplemental Movie 4**). The undegraded velocity of the observed movement for a long distance indicates no effect of the tip-sample interaction on the motor activity. Let us discuss this issue in a way different from that mentioned in Other Factors Limiting Feedback Frequency, above. In this imaging with a scan size of 150×75 nm^2, at 7 fps, we used a cantilever having $f_c \approx 1$ MHz in water, $k_c \approx 0.2$ N/m, and $Q_c \approx 2$ in water. The oscillating cantilever tip therefore taps the sample surface 12.7 times per 1×1 nm^2. As the two-dimensional size of the motor domain is roughly 5×5 nm^2, the motor domain is tapped with the tip ∼320 times during one frame time (1/7 s) and much more (>50,000 times) during the successive imaging, clearly indicating no accumulation but quick dissipation of the energy given to the molecule by the tapping.

In this imaging, the cantilever free oscillation amplitude A_0 and amplitude set point A_s were set at ∼1 nm and $0.8–0.9 A_s$, respectively. On average, the energy of the oscillating cantilever dissipates after every tapping by $1/2 k_c (A_0^2 - A_s^2)/Q_c = 2.3–4.4$ $k_B T$, where T is 300 K. Even when the oscillation energy is completely lost, its energy loss is only 24 $k_B T$ (similar to the energy of ATP hydrolysis, ∼20 $k_B T$). Even if the motor domain is mechanically excited by this amount of energy, the energy would quickly dissipate into many degrees of freedom including those of surrounding water molecules. Thus, so long as small free oscillation amplitude is used for a cantilever with
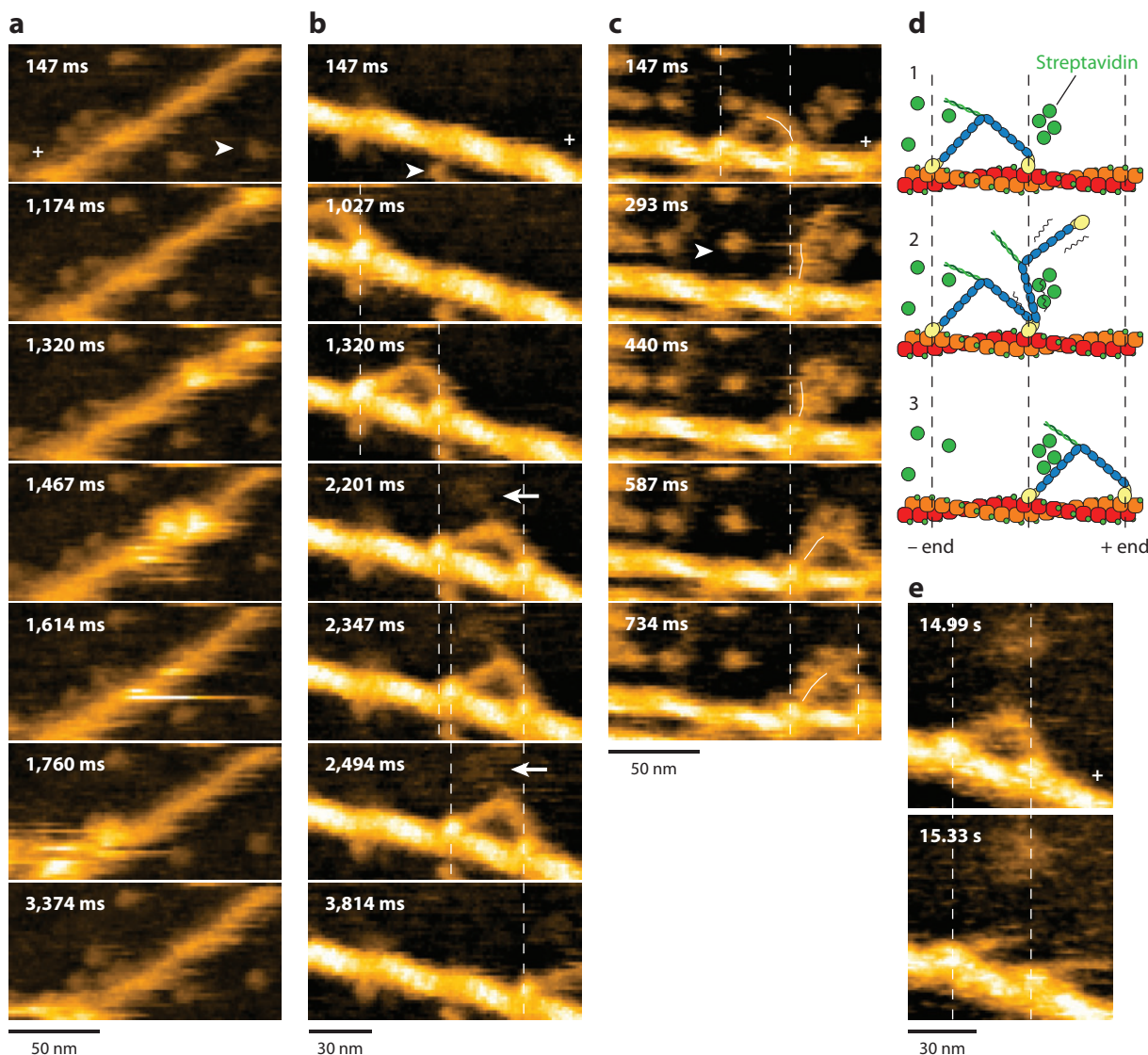
Figure 4

Walking tail-truncated myosin V (M5-HMM) and unfolding of coiled-coil tail captured by high-speed atomic force microscopy (HS-AFM). (*a*) Successive AFM images showing processive movement of M5-HMM in 1 μM ATP when positively charged lipid is absent on the planar lipid bilayer (PLB) surface. Frame rate, 7 fps. (*b*) Successive AFM images showing processive movement of M5-HMM in 1 μM ATP when positively charged lipid is present on the PLB surface. Arrows indicate the coiled-coil tail pointing to the minus end of actin. (*c*) Successive AFM images showing hand-overhand movement in 1 μM ATP. The swinging lever is highlighted with a thin white line. (*d*) Schematic explaining the images in panel *c*. (*e*) Unfolding of the coiled-coil tail of two-headed bound M5-HMM. Top image, before unfolding; bottom image, after unfolding. The symbol "+" indicates the plus ends of actin filaments. The arrowheads show some of streptavidin molecules. Vertical dashed lines show the centers of mass of the motor domains. The frame rates used are 7 fps for panels *a–c* and 3 fps for panel *e*. The z-scales are 18 nm for panel *a* and 10.5 nm for panels *b*, *c*, and *e*. Adapted with permission from Reference 52.

$k_c \approx 0.2$ N/m, the function of M5-HMM (and other proteins) is not disturbed by the oscillating tip even when tapped many times.

Spontaneous swing of leading head in hand-overhand movement. As shown in **Figure 4c** and **Supplemental Movie 3**, after trailing head detachment, the leading head appeared to spontaneously rotate from the reverse arrowhead orientation toward the arrowhead orientation (the term arrowhead originates from the configuration of single-headed myosin bound to an actin filament in the rigor state). Before completing this rotation, the leading head briefly halted by colliding with a streptavidin molecule placed in the way of its natural path, and the detached trailing head was most distant from the actin filament and slightly rotated around the neck-neck junction. Then, the leading head overcame the streptavidin blockade and completely rotated to the arrowhead orientation. Accompanied by this further rotation, the trailing head was bound to a forward site of the actin filament to become a new leading head, completing one step. Here, it was clearly revealed that before the completion of a step, the trailing head never interacted with actin but passively moved forward, driven by the rotating leading head. The rotation of the leading head is exactly the swinging lever arm motion proposed by Huxley (38) for the powerstroke of muscle myosin, a hypothesis that existed for a long time without clinching evidence.

Foot stomp and unwinding of the coiled-coil tail. The seemingly spontaneous rotation of the leading head following trailing head detachment suggests that intramolecular tension for the advance has already existed in the two-headed bound molecule. In this bound state, the trailing head is in the arrowhead orientation, which is natural at least for the ADP-bound or nucleotide-free head. Nevertheless, the leading head is not in the natural orientation (i.e., in the reverse arrowhead orientation) and therefore pays an energy cost to generate the intramolecular tension, which is implied in the slightly curved appearance of the leading head. Upon trailing head detachment, the constraint keeping the bound leading head in the unnatural orientation is removed and hence the leading head spontaneously rotates forward, meaning that the bound leading head is in a strained prestroke state and that the lever arm swing is not accompanied by chemical transitions.

Interestingly, during the two-headed bound state in ATP, the motor domain of the leading head frequently exhibited brief dissociation and reassociation on the same actin filament, whereas the molecule remained at approximately the same position on the filament (**Supplemental Movies 3** and **4**). Similarly, the motor domain of the trailing head exhibited a brief translocation by $\sim \pm 5$ nm along the actin filament. We termed these behaviors foot stomp. The foot stomp was observed more frequently at the leading head than at the trailing head (approximately 3:1). Although not well documented, a foot-stomp-like behavior was previously suggested in fluorescence microscopy observations of walking myosin V molecules (89, 95). Thus, the foot stomp is an inherent behavior of myosin V.

The foot stomp at the leading head seems to raise an important issue of the chemomechanical coupling in this motor. The briefly detached leading head does not carry bound Pi because Pi release occurs immediately after the initial binding of the ADP–Pi-bound head to actin (21). Nevertheless, the detached leading head with only ADP bound rebinds to actin still in the reverse arrowhead orientation, and then swings forward following trailing head detachment, indicating that tension generation for forward movement can occur without transitioning through an ADP–Pi-bound state. It can occur in the ADP-bound state. Thus, the tension generation for forward movement does not seem to require that chemical energy be supplied by ATP hydrolysis.

During the two-headed bound state in ADP, the short coiled-coil tail was sometimes unwound, immediately after which the monomerized leading head rotated toward the arrowhead orientation, similar to the swinging lever arm (**Figure 4e**). Again, this unwinding suggests that the distortion

of the actin-bound leading head, which does not require chemical energy, is the source of the intramolecular tension generation for forward movement.

Mechanism of hand-overhand movement. The leading head of two-headed bound M5-HMM was straight (slightly curved outward) in ADP or ATP, whereas it was often sharply bent in the nucleotide-free condition. Therefore, the conformation of the leading head indicates whether the leading head contains nucleotides. From AFM movies of actin-bound M5-HMM in various concentrations of ADP, the ADP dissociation rate constant at the leading head was estimated to be 0.1 s^{-1}. Thus, ADP is released from the leading head every 10 s, on average. However, M5-HMM walks many steps for 10 s, meaning that ADP does not dissociate from the leading head. ADP dissociation, the subsequent ATP binding, and the resulting detachment from actin solely occur at the trailing head. This is the basis underlying the processive hand-overhand movement. This mechanism was inferred previously from various indirect experiments (27, 70, 73, 75, 78, 102) but is now clearly and directly demonstrated by the HS-AFM observation.

Rotary Catalysis of Rotorless F_1-ATPase

The $\alpha_3\beta_3\gamma$ subcomplex of F_1-ATPase (a part of ATP synthase) is the minimum complex for the full ATPase activity. About half the length of the long γ subunit is inserted into the central cavity formed by a ring-shaped $\alpha_3\beta_3$ where three α subunits and three β subunits are arranged alternately (1). Three ATP binding sites locate at the α-β interfaces, mainly in the β subunits. The $\alpha_3\beta_3\gamma$ subcomplex is a rotary motor (34, 48, 68, 115) (**Figure 5a**). The γ subunit rotates in the stator $\alpha_3\beta_3$ ring driven by rotary hydrolysis of ATP at the three β subunits. The rotation occurs in the counterclockwise direction as viewed from the exposed side of the γ subunit (or from the C-terminal side of $\alpha_3\beta_3$). In the ATPase cycle, three β subunits take different chemical states: ATP-bound, ADP-bound, and nucleotide-free (empty) states (1, 34). Each chemical state cyclically propagates over the three β subunits. Thus, there is strong cooperativity between β subunits.

How is the cooperativity essential for torque generation to rotate the γ subunit engendered without direct contact between the β subunits? In every instance, the β-γ interaction is different among the three β subunits because the γ subunit has no symmetry. In consideration of this fact, it was proposed that interactions with the γ subunit control the conformational and catalytic states of individual β subunits (105). This idea was reinforced by studies showing that backward mechanical rotation of the γ subunit with external force reverses the chemical reaction toward ATP synthesis (42, 74), whereas forced forward rotation results in accelerated ATP binding (41). This view was challenged by the finding that even when the γ subunit is shortened so that most γ-β interaction sites are abolished, the short γ subunit still rotates unidirectionally (30, 62). However, because single-molecule optical microscopy requires attachment of a probe to the γ subunit for the observation of rotary catalysis, it cannot examine whether the rotary catalysis (hence, the cooperativity) occurs with $\alpha_3\beta_3$ alone. This issue was solved by HS-AFM imaging of $\alpha_3\beta_3$ in ATP (99), as described below.

HS-AFM imaging of $\alpha_3\beta_3$ subcomplex. $\alpha_3\beta_3$ with Lys_7-tags at the N termini of the β subunits was covalently immobilized to a mica surface that was first coated with 3-aminopropyl-triethoxysilane and then treated with glutaraldehyde. An image of the C-terminal side of $\alpha_3\beta_3$ without nucleotide shows a pseudo-sixfold symmetric ring (**Figure 5b**). Each subunit has an upwardly protruding portion at the inner top side of the ring, but these portions are higher at three alternately arranged subunits than at the other three. When this image was compared with a simulated AFM image (**Figure 5d**) constructed from a crystal structure of nucleotide-free $\alpha_3\beta_3$ (PDB
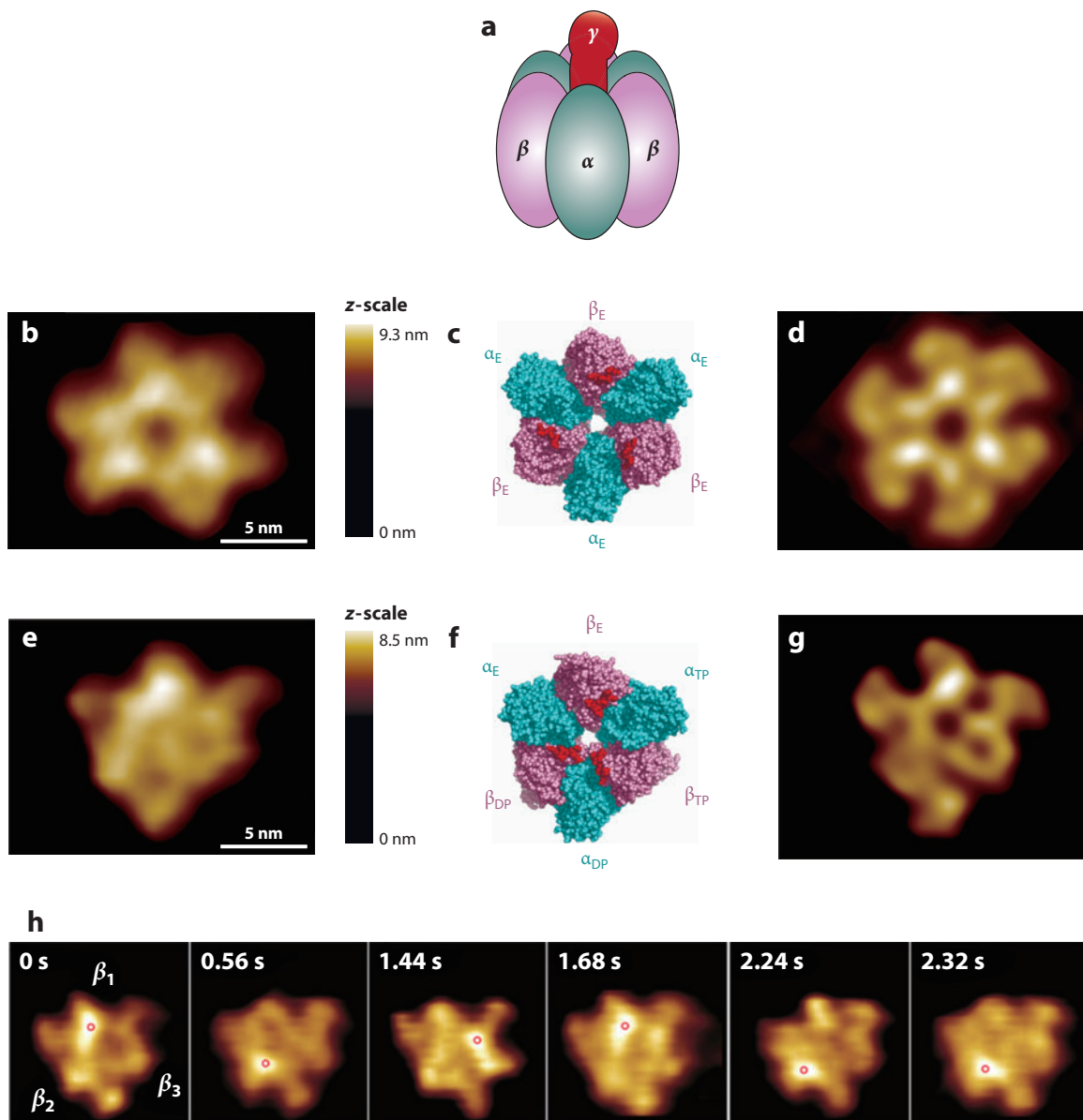
Figure 5

Atomic force microscopy (AFM) images of the $\alpha_3\beta_3$ subcomplex at the C-terminal surface. (*a*) Schematic for F_1-ATPase. (*b*) Averaged AFM image obtained in nucleotide-free condition. (*c*) The C-terminal surface of crystal structure of a nucleotide-free $\alpha_3\beta_3$ subcomplex. (*d*) Simulated AFM image of panel *c*. (*e*) Averaged AFM image obtained in 1-mM AMP-PNP. (*f*) The C-terminal surface of crystal structure of an $\alpha_3\beta_3$ subcomplex obtained in ATP. (*g*) Simulated AFM image of panel *f*. (*h*) Successive AFM images showing counterclockwise rotary propagation of conformational change of an $\alpha_3\beta_3$ subcomplex at the C-terminal surface captured by high-speed AFM in the presence of 2 μM ATP, at 12.5 fps. The red circle marks the highest pixel position in each image. The color scale placed at the right-hand side of panels *b* and *e* indicate the *z*-scale for the respective images. Adapted with permission from Reference 99.

ID: 1SKY) (88) (**Figure 5c**), the three subunits showing higher protrusions were identified as β subunits.

In 1 mM AMP-PNP, the shape of $\alpha_3\beta_3$ became triangular and the central hole became obscure (**Figure 5e**). Only one subunit had a higher protrusion and an outwardly extended distal portion. This is very likely to be a β subunit. If so, two subunits whose distal parts are retracted toward the center are β subunits, in consideration of the alternate subunit arrangement. This assignment was confirmed by the comparison of the AFM image and a simulated AFM image (**Figure 5g**) constructed using a crystal structure of a nucleotide-bound $\alpha_3\beta_3\gamma$ subcomplex (PDB ID: 1BMF) (1) from which the γ subunit was removed (**Figure 5f**). In addition, it was clarified that the β subunit with the highest protrusion and an extended distal portion is empty and that the two β subunits with retracted distal portions are nucleotide bound.

When imaged in 2–4 μM ATP at 12.5 fps, distinct conformational dynamics appeared at the β subunits (**Figure 5h**; **Supplemental Movie 5**). Each β subunit exhibited a conformational ▶ Supplemental Material transition between the outwardly extended high state (open, O, state) and the retracted low state (closed, C, state). The following prominent features were observed: (*a*) Only one β subunit assumes the O state as in the presence of AMP-PNP, and (*b*) when the O-to-C transition occurs at one β subunit, the opposite C-to-O transition occurs simultaneously at its counterclockwise neighbor β subunit in most cases. Thus, the O conformation propagates counterclockwise (**Figure 5h**, red circles). The ATP hydrolysis rates at 2, 3, and 4 μM ATP were in approximate agreement with the rates of conformational revolution at 2, 3, and 4 μM ATP, respectively.

These dynamic transitions indicate that the O-to-C transition occurs when ATP is bound to an empty β subunit and that the C-to-O transition occurs when an ADP-bound β subunit releases ADP. So, the empty, ADP-bound, and ATP-bound β subunits are arranged counterclockwise in this order, and therefore, the observed conformational propagation demonstrates rotary catalysis by the $\alpha_3\beta_3$ subcomplex. Thus, we reach the most important conclusion: The intrinsic cooperativity responsible for torque generation to rotate the γ subunit is elicited through β-β interplay alone and the γ subunit passively undergoes torque to rotate (99).

FUTURE CHALLENGES

As exemplified by these imaging studies, HS-AFM can provide high-resolution movies of biological molecules in action from which we can learn a great detail about how the molecules operate to function. However, current HS-AFM has the following limitations: (*a*) The scan range of the high-speed scanner is limited to 1 μm, 4 μm, and 1 μm in the *x*-, *y*-, and *z*-directions, respectively, to achieve high resonant frequencies for fast scan, and (*b*) because the cantilever tip makes contact with the sample, very soft surfaces such as the membranes of live eukaryotic cells are largely deformed by the contact, which disables the visualization of molecules on such soft surfaces. Below, we describe ongoing and future endeavors to overcome these limitations.

Wide-Area Observation and In Situ Imaging of Dynamic Processes

The size of a wider-area scanner becomes larger, resulting in lower resonant frequencies and hence a lower highest-possible scan speed. This adverse effect has been recently removed by a simple inversion-based feedforward control technique (7) and by an enhanced iterative inverse control technique (54, 114). Therefore, even with a scanner capable of scanning over $\sim40 \times 40$ μm^2, a line scan of ~100 Hz is now possible without production of vibrations. However, because these inverse control techniques capable of extending the bandwidth cannot be applied to the *z*-scanner,

its bandwidth is still limited. Nonetheless, a large sample such as a live eukaryotic cell can now be imaged within ~60 s when a relatively small number of scan lines (~200) are used.

After taking a whole topography image of a large biological sample, we can image molecules in a local area of interest on the sample surface when the surface is relatively rigid. For example, it is possible to observe dynamics of molecules on the surfaces of live bacterial cells, intracellular organelles (such as mitochondria and nuclei), and small structures such as neuronal spines. In fact, in situ visualization of porin trimers moving on the outer surface of a live magnetic bacterium was recently accomplished (112). Such in situ dynamic molecular imaging will have a great impact on cell biology because dynamic molecular processes occurring on these surfaces are largely unknown.

Faster Wide-Area Observation and Dynamic Imaging of Cell Morphology

For the imaging of a whole cell, many-pixel images with single-nanometer resolution are unnecessary. Nonetheless, in the tapping mode, the feedback operation has to be continuously performed for a huge number of points on the surface; thus, it takes a long time to image a whole cell. This situation can be improved by the use of a different operation mode employed by scanning ion conductance microscopy (SICM). This mode, called AC mode (71), pulse mode (36, 55), or hopping mode (69), has been devised to avoid probe-sample collision; a probe (glass capillary) is moved up and down during lateral scanning of the sample stage. Therefore, the feedback operation is discretely carried out only at lateral positions where the sample height information is acquired. Its imaging acquisition time is given by the number of pixels contained in an image divided by the up-and-down frequency f_{ud}. With $f_{ud} = 20$ kHz, a 50×50 μm^2 image with 250×250 pixels can be acquired within approximately 3 s. The resonant frequency of commercially available stack piezoactuators displaceable up to 10 μm is approximately 30 kHz when their ends on one side are fixed. Therefore, this image acquisition time is realistic as far as the sample stage can be quickly retracted upon tip-sample contact.

High-Speed Noncontact Imaging

A noncontact condition is mandatory for visualizing molecules on the extremely soft surfaces of eukaryotic cells. SICM has already achieved this condition (16, 35). With the use of very sharp glass capillaries with a small pore at the apex, the spatial resolution of SICM has reached a few nanometers (117). Immobile protein molecules with a size of ~14 nm in live cell membranes have been successfully imaged (84). Moreover, not only imaging but also smart electrophysiological measurements are possible with SICM (59). However, the bandwidth of ion conductivity detection is low, because of the high impedance to ionic current through the small pore of a capillary electrode and because of slow ionic currents. But, there is a possibility of increasing the bandwidth. Scanning tunneling microscopy also has a high impedance (hence a low bandwidth) problem but it has already been overcome by a circuitry technique (45). The slow ionic current problem can be solved by the positioning of the counter-electrode close to the capillary end.

Noncontact AFM called solution-vibration AFM is currently being developed by the Ando group. The sample stage is vibrated at a high frequency (1–3 MHz) with small amplitude, which in turn vibrates the sample solution placed on the top of the sample stage. Although the vibrations are transmitted to a place far from the sample surface, only solution vibrations at places in close proximity to the sample surface are affected by the presence of the sample. In fact, when the tip end was close to the surface of a polystyrene bead with a diameter of 150 nm (at a distance of <50 nm), the bead was visualized clearly by the phase detection of the cantilever vibrations (H. Watanabe, T. Saito & T. Ando, unpublished result).

SUMMARY POINTS

1. Using HS-AFM, we can directly observe the structure dynamics and dynamic processes of biomolecules, at subsecond to sub-100-ms temporal and submolecular spatial resolution, without disturbing their function.

2. Visualized dynamic images of biomolecules can provide information inaccessible with other approaches, giving great insight into how the molecules function.

3. Dynamics of molecules that appear in AFM movies can be interpreted straightforwardly without intricate analyses and interpretations, making it possible to attain firm conclusions.

4. In situ dynamic imaging of biomolecules is now becoming possible.

5. HS-AFM will transform structural biology and single-molecule biophysics.

DISCLOSURE STATEMENT

The authors are not aware of any affiliations, memberships, funding, or financial holdings that might be perceived as affecting the objectivity of this review.

ACKNOWLEDGMENTS

LITERATURE CITED

1. Abrahams JP, Leslie AG, Lutter R, Walker JE. 1994. Structure at 2.8 Å resolution of F_1-ATPase from bovine heart mitochondria. *Nature* 370:621–28

2. Albrecht TR, Grütter P, Horne D, Rugar D. 1991. Frequency modulation detection using high-Q cantilevers for enhanced force microscope sensitivity. *J. Appl. Phys.* 69:668–73

3. **Ando T. 2012. High-speed atomic force microscopy coming of age. *Nanotechnology* 23:062001**

4. Ando T, Kodera N, Maruyama D, Takai E, Saito K, et al. 2002. A high-speed atomic force microscope for studying biological macromolecules in action. *Jpn. J. Appl. Phys.* 41:4851–56

5. **Ando T, Kodera N, Takai E, Maruyama D, Saito K, et al. 2001. A high-speed atomic force microscope for studying biological macromolecules. *Proc. Natl. Acad. Sci. USA* 98:12468–72**

6. Ando T, Uchihashi T. 2012. High-speed AFM and imaging of biomolecular processes. In *Nanoscale Liquid Interfaces: Wetting, Patterning and Force Microscopy at Molecular Scale*, ed. T Ondarçuhu, JP Aimé, pp. 711–40. Singapore: Pan Stanford Publ.

7. **Ando T, Uchihashi T, Fukuma T. 2008. High-speed atomic force microscopy for nano-visualization of dynamic biomolecular processes. *Prog. Surf. Sci.* 83:337–437**

8. Ando T, Uchihashi T, Kodera N, Miyagi A, Nakakita R, et al. 2005. High-speed AFM for studying the dynamic behavior of protein molecules at work. *e-J. Surf. Sci. Nanotechnol.* 3:384–92

9. Ando T, Uchihashi T, Kodera N, Miyagi A, Nakakita R, et al. 2006. High-speed atomic force microscopy for studying the dynamic behavior of protein molecules at work. *Jpn. J. Appl. Phys.* 45:1897–903

10. Binnig G, Quate CF, Gerber C. 1986. Atomic force microscope. *Phys. Rev. Lett.* 56:930–33

11. Blankenburg R, Meller P, Ringsdorf H, Salesse C. 1989. Interaction between biotin lipids and streptavidin in monolayers: formation of oriented two-dimensional protein domains induced by surface recognition. *Biochemistry* 28:214–21

3. Reviews various bioimaging studies by high-speed AFM.

5. Presents first high-speed AFM, capturing moving protein molecules at 12.5 fps.

7. Extensively reviews various techniques leading to the establishment of high-speed AFM for biological studies.

12. Casuso I, Khao J, Chami M, Paul-Gilloteaux P, Husain M, et al. 2012. Characterization of the motion of membrane proteins using high-speed atomic force microscopy. *Nat. Nanotechnol.* 7:525–29

13. Casuso I, Kodera N, Le Grimellec C, Ando T, Scheuring S. 2009. High-resolution high-speed contact mode atomic force microscopy movies of purple membrane. *Biophys. J.* 97:1354–61

14. Casuso I, Rico F, Scheuring S. 2011. High-speed atomic force microscopy: structure and dynamics of single proteins. *Curr. Opin. Chem. Biol.* 15:704–9

15. Casuso I, Sens P, Rico F, Scheuring S. 2010. Experimental evidence for membrane-mediated protein-protein interaction. *Biophys. J.* 99:L47–49

16. Chen C-C, Zhou Y, Baker LA. 2012. Scanning ion conductance microscopy. *Annu. Rev. Anal. Chem.* 5:207–28

17. Costa LT, Pinto JR, Moraes MB, de Souza GGB, Sorenson MM, et al. 2004. Chemical treatment of mica for atomic force microscopy can affect biological sample conformation. *Biophys. Chem.* 109:63–71

18. Czajkowsky DM, Shao Z. 2003. Inhibition of protein adsorption to muscovite mica by monovalent cations. *J. Microsc.* 211:1–7

19. Dague E, Alsteens D, Latgé J-P, Verbelen C, Raze D, et al. 2007. Chemical force microscopy of single live cells. *Nano Lett.* 7:3026–30

20. Darst SA, Ahlers M, Meller PH, Kubalek EW, Blankenburg R, et al. 1991. Two-dimensional crystals of streptavidin on biotinylated lipid layers and their interactions with biotinylated macromolecules. *Biophys. J.* 59:387–96

21. De La Cruz EM, Wells AL, Rosenfeld SS, Ostap EM, Sweeney HL. 1999. The kinetic mechanism of myosin V. *Proc. Natl. Acad. Sci. USA* 96:13726–31

22. Endo M, Hidaka K, Sugiyama H. 2011. Direct AFM observation of an opening event of a DNA cuboid constructed via a prism structure. *Org. Biomol. Chem.* 9:2075–77

23. Endo M, Katsuda Y, Hidaka K, Sugiyama H. 2010. Regulation of DNA methylation using different tensions of double strands constructed in a defined DNA nanostructure. *J. Am. Chem. Soc.* 132:1592–97

24. Fantner GE, Hegarty P, Kindt JK, Schitter G, Cidade GAG, et al. 2005. Data acquisition system for high speed atomic force microscopy. *Rev. Sci. Instrum.* 76:026118

25. Fantner GE, Schitter G, Kindt JH, Ivanov T, Ivanova K, et al. 2006. Components for high speed atomic force microscopy. *Ultramicroscopy* 106:881–87

26. Fernandez JM, Li H. 2004. Force-clamp spectroscopy monitors the folding trajectory of a single protein. *Science* 303:1674–78

27. Forgacs E, Cartwright S, Sakamoto T, Sellers JR, Corrie JE, et al. 2008. Kinetics of ADP dissociation from the trail and lead heads of actomyosin V following the power stroke. *J. Biol. Chem.* 283:766–73

28. Forkey JN, Quinlan ME, Shaw MA, Corrier JET, Goldman YE. 2003. Three-dimensional structural dynamics of myosin V by single-molecule fluorescence polarization. *Nature* 422:399–404

29. Fukuma T, Okazaki Y, Kodera N, Uchihashi T, Ando T. 2008. High resonance frequency force microscope scanner using inertia balance support. *Appl. Phys. Lett.* 92:243119

30. Furuike S, Hossain MD, Maki Y, Adachi K, Suzuki T, et al. 2008. Axle-less F_1-ATPase rotates in the correct direction. *Science* 319:955–58

31. Gan Y. 2009. Atomic and subnanometer resolution in ambient conditions by atomic force microscopy. *Surf. Sci. Rep.* 64:99–121

32. Gilmore JL, Suzuki Y, Tamulaitis G, Siksnys V, Takeyasu K, et al. 2009. Single-molecule dynamics of the DNA−*Eco*RII protein complexes revealed with high-speed atomic force microscopy. *Biochemistry* 48:10492–98

33. Giocondi M-C, Yamamoto D, Lesniewska E, Milhiet P-E, Ando T, et al. 2010. Surface topography of membrane domains. *Biochim. Biophys. Acta* 1798:703–18

34. Gresser MJ, Myers JA, Boyer PD. 1982. Catalytic site cooperativity of beef heart mitochondrial F_1 adenosine triphosphatase. Correlations of initial velocity, bound intermediate, and oxygen exchange measurements with an alternating three-site model. *J. Biol. Chem.* 257:12030–38

35. Hansma PK, Drake B, Marti O, Gould SA, Prater CB. 1989. The scanning ion-conductance microscope. *Science* 243:641–43

36. Happel P, Hoffmann G, Mann SA, Dietzel ID. 2003. Monitoring cell movements and volume changes with pulse-mode scanning ion conductance microscopy. *J. Microsc.* 212:144–51

37. Hinterdorfer P, Dufrêne YF. 2006. Detection and localization of single molecular recognition events using atomic force microscopy. *Nat. Methods* 3:347–55

38. Huxley HE. 1969. The mechanism of muscular contraction. *Science* 164:1356–66

39. Igarashi K, Koivula A, Wada M, Kimura S, Penttilä M, Samejima M. 2009. High speed atomic force microscopy visualizes processive movement of *Trichoderma reesei* cellobiohydrolase I on crystalline cellulose. *J. Biol. Chem.* 284:36186–90

40. Igarashi K, Uchihashi T, Koivula A, Wada M, Kimura S, et al. 2011. Traffic jams reduce hydrolytic efficiency of cellulase on cellulose surface. *Science* 333:1279–82

41. Iko Y, Tabata KV, Sakakihara S, Nakashima T, Noji H. 2009. Acceleration of the ATP-binding rate of F_1-ATPase by forcible forward rotation. *FEBS Lett.* 583:3187–91

42. Itoh H, Takahashi A, Adachi K, Noji H, Yasuda R, et al. 2004. Mechanically driven ATP synthesis by F_1-ATPase. *Nature* 427:465–68

43. Jonkheijm P, Weinrich D, Schröder H, Niemeyer CM, Waldmann H. 2008. Chemical strategies for generating protein biochips. *Angew. Chem. Int. Ed.* 47:9618–47

44. Katan AJ, Dekker C. 2011. Leading edge, minireview: high-speed AFM reveals the dynamics of single biomolecules at the nanometer scale. *Cell* 147:979–82

45. Kemiktarak U, Ndukum T, Schwab KC, Ekinci KL. 2007. Radio-frequency scanning tunneling microscopy. *Nature* 450:85–88

46. Kim J, Kim G, Cremer PS. 2001. Investigations of water structure at the solid/liquid interface in the presence of supported lipid bilayers by vibrational sum frequency spectroscopy. *Langmuir* 17:7255–60

47. Kindt JH, Fantner GE, Cutroni JA, Hansma PK. 2004. Rigid design of fast scanning probe microscopes using finite element analysis. *Ultramicroscopy* 100:259–65

48. Kinosita K Jr, Adachi K, Itoh H. 2004. Rotation of F_1-ATPase: how an ATP-driven molecular machine may work. *Annu. Rev. Biophys. Biomol. Struct.* 33:245–68

49. Kitazawa M, Ohta R, Okita T, Tanaka J, Tanemura M. 2007. Mechanical properties of single carbon nanofibers grown on tips of scanning probe microscopy cantilevers by ion irradiation. *Jpn. J. Appl. Phys.* 46:6324–28

50. Kitazawa M, Shiotani K, Toda A. 2003. Batch fabrication of sharpened silicon nitride tips. *Jpn. J. Appl. Phys.* 42:4844–47

51. Kodera N, Sakashita M, Ando T. 2006. Dynamic proportional-integral-differential controller for high-speed atomic force microscopy. *Rev. Sci. Instrum.* 77:083704

52. Kodera N, Yamamoto D, Ishikawa R, Ando T. 2010. Video imaging of walking myosin V by high-speed atomic force microscopy. *Nature* 468:72–76

53. Kodera N, Yamashita H, Ando T. 2005. Active damping of the scanner for high-speed atomic force microscopy. *Rev. Sci. Instrum.* 76:053708

54. Li Y, Bechhoefer J. 2009. Model-free iterative control of repetitive dynamics for high-speed scanning in atomic force microscopy. *Rev. Sci. Instrum.* 80:013702

55. Mann SA, Hoffmann G, Hengstenberg A, Schuhmann W, Dietzel ID. 2002. Pulse-mode scanning ion conductance microscopy—a method to investigate cultured hippocampal cells. *J. Neurosci. Methods* 116:113–17

56. Mehta AD, Rock RS, Rief M, Spudich JA, Mooseker MS, et al. 1999. Myosin-V is a processive actin-based motor. *Nature* 400:590–93

57. Milhiet PE, Yamamoto D, Berthoumieu O, Dosset P, Le Grimellec C, et al. 2010. Deciphering the structure, growth and assembly of amyloid-like fibrils using high-speed atomic force microscopy. *PLoS ONE* 5:e13240

58. Mingeot-Leclercq M-P, Deleu M, Brasseur R, Dufrêne YF. 2008. Atomic force microscopy of supported lipid bilayers. *Nat. Protoc.* 3:1654–59

59. Miragoli M, Moshkov A, Novak P, Shevchuk A, Nikolaev VO, et al. 2011. Scanning ion conductance microscopy: a convergent high-resolution technology for multi-parametric analysis of living cardiovascular cells. *J. R. Soc. Interface* 8:913–25

60. Miyagi A, Ando T, Lyubchenko YL. 2011. Dynamics of nucleosomes assessed with time-lapse high-speed atomic force microscopy. *Biochemistry* 50:7901–8

51. Presents a new feedback controller that solves the difficult parachuting problem.

52. Presents astonishing AFM movies of myosin V walking on actin filament.

61. Miyagi A, Tsunaka Y, Uchihashi T, Mayanagi K, Hirose S, et al. 2008. Visualization of intrinsically disordered regions of proteins by high-speed atomic force microscopy. *Chem. Phys. Chem.* 9:1859–66

62. Mnatsakanyan N, Krishnakumar AM, Suzuki T, Weber J. 2009. The role of the βDELSEED-loop of ATP synthase. *J. Biol. Chem.* 284:11336–45

63. Moreno-Herrero F, Colchero F, Gómez-Herrero J, Baró AM. 2004. Atomic force microscopy contact, tapping, and jumping modes for imaging biological samples in liquids. *Phys. Rev. E* 69:031915

64. Müller DJ, Dufrêne YF. 2008. Atomic force microscopy as a multifunctional molecular toolbox in nanobiotechnology. *Nat. Nanotechnol.* 3:261–69

65. Müller DJ, Helenius J, Alsteens D, Dufrêne YF. 2009. Force probing surfaces of living cells to molecular resolution. *Nat. Chem. Biol.* 5:383–90

66. Müller DJ, Janovjak H, Lehto T, Kuerschner L, Anderson K. 2002. Observing structure, function and assembly of single proteins by AFM. *Prog. Biophys. Mol. Biol.* 79:1–43

67. Nakajima H, Kunioka Y, Nakano K, Shimizu K, Seto M, et al. 1997. Scanning force microscopy of the interaction events between a single molecule of heavy meromyosin and actin. *Biochem. Biophys. Res. Commun.* 234:178–82

68. Noji H, Yasuda R, Yoshida M, Kinosita K Jr. 1997. Direct observation of the rotation of F_1-ATPase. *Nature* 386:299–302

69. Novak P, Li C, Shevchuk AI, Stepanyan R, Caldwell M, et al. 2009. Nanoscale live-cell imaging using hopping probe ion conductance microscopy. *Nat. Methods* 6:279–81

70. Oguchi Y, Mikhailenko SV, Ohki T, Olivares AO, De La Cruz EM, Ishiwata S. 2008. Load-dependent ADP binding to myosins V and VI: implications for subunit coordination and function. *Proc. Natl. Acad. Sci. USA* 105:7714–19

71. Pastré D, Iwamoto H, Liu J, Szabo G, Shao Z. 2001. Characterization of AC mode scanning ion-conductance microscopy. *Ultramicroscopy* 90:13–19

72. Pastré D, Piétrement O, Fusil S, Landousy F, Jeusset J, et al. 2003. Adsorption of DNA to mica mediated by divalent counterions: a theoretical and experimental study. *Biophys. J.* 85:2507–18

73. Purcell TJ, Sweeney HL, Spudich JA. 2005. A force-dependent state controls the coordination of processive myosin V. *Proc. Natl. Acad. Sci. USA* 102:13873–78

74. Rondelez Y, Tresset G, Nakashima T, Kato-Yamada Y, Fujita H, et al. 2005. Highly coupled ATP synthesis by F_1-ATPase single molecules. *Nature* 433:773–77

75. Rosenfeld SS, Sweeney HL. 2004. A model of myosin V processivity. *J. Biol. Chem.* 279:40100–11

76. Sackmann E. 1996. Supported membranes: scientific and practical applications. *Science* 271:43–48

77. Sakamoto T, Amitani I, Yokota E, Ando T. 2000. Direct observation of processive movement by individual myosin V molecules. *Biochem. Biophys. Res. Commun.* 272:586–90

78. Sakamoto T, Webb MR, Forgacs E, White HD, Sellers JR. 2008. Direct observation of the mechanochemical coupling in myosin Va during processive movement. *Nature* 455:128–32

79. Sanchez H, Suzuki Y, Yokokawa M, Takeyasu K, Wyman C. 2011. Protein-DNA interactions in high speed AFM: single molecule diffusion analysis of human RAD54. *Integr. Biol.* 3:1127–34

80. Sannohe Y, Endo M, Katsuda Y, Hidaka K, Sugiyama H. 2010. Visualization of dynamic conformational switching of the G-quadruplex in a DNA nanostructure. *J. Am. Chem. Soc.* 132:16311–13

81. Scheuring S, Fotiadis D, Möller C, Müller SA, Engel A, et al. 2001. Single proteins observed by atomic force microscopy. *Single Mol.* 2:59–67

82. Scheuring S, Sturgis JN. 2005. Chromatic adaptation of photosynthetic membranes. *Science* 309:484–87

83. Sellers JR, Weisman LS. 2008. Myosin V. In *Myosins: A Superfamily of Molecular Motors*, Vol. 7: *Proteins and Cell Regulation*, ed. LM Coluccio, pp. 289–323. Berlin: Springer. 482 pp.

84. Shevchuk AI, Frolenkov GI, Sanchez D, James PS, Freedman N, et al. 2006. Imaging proteins in membranes of living cells by high-resolution scanning ion conductance microscopy. *Angew. Chem. Int. Ed.* 45:2212–16

85. Shibata M, Uchihashi T, Yamashita H, Kandori H, Ando T. 2011. Structural changes in bacteriorhodopsin in response to alternate illumination observed by high-speed atomic force microscopy. *Angew. Chem. Int. Ed.* 50:4410–13

86. **Shibata M, Yamashita H, Uchihashi T, Kandori H, Ando T. 2010. High-speed atomic force microscopy shows dynamic molecular processes in photo-activated bacteriorhodopsin. *Nat. Nanotechnol.* 5:208–12**

87. Shinozaki Y, Sumitomo K, Tsuda M, Koizumi S, Inoue K, et al. 2009. Direct observation of ATP-induced conformational changes in single P2X$_4$ receptors. *PLoS Biol.* 7:e1000103

88. Shirakihara Y, Leslie AG, Abrahams JP, Walker JE, Ueda T, et al. 1997. The crystal structure of the nucleotide-free α3β3 subcomplex of F$_1$-ATPase from the thermophilic *Bacillus* PS3 is a symmetric trimer. *Structure* 5:825–36

89. Shiroguchi K, Kinosita K Jr. 2007. Myosin V walks by lever action and Brownian motion. *Science* 316:1208–12

90. Stewart MP, Helenius J, Toyoda Y, Ramanathan SP, Müller DJ, et al. 2011. Hydrostatic pressure and the actomyosin cortex drive mitotic cell rounding. *Nature* 469:226–30

91. Stroh C, Wang H, Bash R, Ashcroft B, Nelson J, et al. 2004. Single-molecule recognition imaging microscopy. *Proc. Natl. Acad. Sci. USA* 101:12503–7

92. Sulchek T, Yaralioglu GG, Quate CF, Minne SC. 2002. Characterization and optimization of scan speed for tapping-mode atomic force microscopy. *Rev. Sci. Instrum.* 73:2928–36

93. Suzuki Y, Gilmore JL, Yoshimura SH, Henderson RM, Lyubchenko YL, et al. 2011. Visual analysis of concerted cleavage by type IIF restriction enzyme SfiI in subsecond time region. *Biophys. J.* 101:2992–98

94. Suzuki Y, Higuchi Y, Hizume K, Yokokawa M, Yoshimura SH, et al. 2010. Molecular dynamics of DNA and nucleosomes in solution studied by fast-scanning atomic force microscopy. *Ultramicroscopy* 110:682–88

95. Syed S, Snyder GE, Franzini-Armstrong C, Selvin PR, Goldman YE. 2006. Adaptability of myosin V studied by simultaneous detection of position and orientation. *EMBO J.* 25:1795–803

96. Tanaka F, Mochizuki T, Liang X, Asanuma H, Tanaka S, et al. 2010. Robust and photocontrollable DNA capsules using azobenzenes. *Nano Lett.* 10:3560–65

97. Tanemura M, Okita T, Yamauchi H, Tanemura S, Morishima R. 2004. Room-temperature growth of a carbon nanofiber on the tip of conical carbon protrusions. *Appl. Phys. Lett.* 84:3831–33

98. Touhami A, Nysten B, Dufrêne YF. 2003. Nanoscale mapping of the elasticity of microbial cells by atomic force microscopy. *Langmuir* 19:4539–43

99. **Uchihashi T, Iino R, Ando T, Noji H. 2011. High-speed atomic force microscopy reveals rotary catalysis of rotorless F$_1$-ATPase. *Science* 333:755–58**

100. Uchihashi T, Kodera N, Ando T. 2012. Guide to video recording of structure dynamics and dynamic processes of proteins by high-speed atomic force microscopy. *Nat. Protoc.* 7:1193–206

101. Uchihashi T, Yamashita H, Ando T. 2006. Fast phase imaging in liquids using a rapid scan atomic force microscope. *Appl. Phys. Lett.* 89:213112

102. Veigel C, Schmitz S, Wang F, Sellers JR. 2005. Load-dependent kinetics of myosin-V can explain its high processivity. *Nat. Cell. Biol.* 7:861–69

103. Viani MB, Pietrasanta LI, Thompson JB, Chand A, Gebeshuber IC, et al. 2000. Probing protein–protein interactions in real time. *Nat. Struct. Biol.* 7:644–47

104. Viani MB, Schäffer TE, Paloczi GT, Pietrasanta LI, Smith BL, et al. 1999. Fast imaging and fast force spectroscopy of single biopolymers with a new atomic force microscope designed for small cantilevers. *Rev. Sci. Instrum.* 70:4300

105. Wang H, Oster G. 1998. Energy transduction in the F$_1$ motor of ATP synthase. *Nature* 396:279–82

106. Warshaw DM, Kennedy GG, Work SS, Krementsova EB, Beck S, et al. 2005. Differential labeling of myosin V heads with quantum dots allows direct visualization of hand-over-hand processivity. *Biophys. J.* 88:L30–32

107. Wickham FJS, Endo M, Katsuda Y, Hidaka K, Bath J, et al. 2011. Direct observation of stepwise movement of a synthetic molecular transporter. *Nat. Nanotechnol.* 6:166–69

108. Williams M, Fowler SB, Robert B, Best RB, Toca-Herrera JL, et al. 2003. Hidden complexity in the mechanical properties of titin. *Nature* 422:446–49

109. Yamamoto D, Nagura N, Omote S, Taniguchi M, Ando T. 2009. Streptavidin 2D crystal substrates for visualizing biomolecular processes by atomic force microscopy. *Biophys. J.* 97:2358–67

86. Presents AFM movies showing bR in response to light and cooperativity by bR-bR interactions.

99. Presents AFM movies showing rotary propagation of conformational changes of rotorless F$_1$-ATPase.

110. Yamamoto D, Uchihashi T, Kodera N, Ando T. 2008. Anisotropic diffusion of point defects in a two-dimensional crystal of streptavidin observed by high-speed atomic force microscopy. *Nanotechnology* 19:384009

111. Yamamoto D, Uchihashi T, Kodera N, Yamashita H, Nishikori S, et al. 2010. High-speed atomic force microscopy techniques for observing dynamic biomolecular processes. *Methods Enzymol.* 457:B541–44

112. Yamashita H, Taoka A, Uchihashi T, Asano T, Ando T, et al. 2012. Single molecule imaging on living bacterial cell surface by high-speed AFM. *J. Mol. Biol.* 422:300–9

113. Yamashita H, Voïtchovsky K, Uchihashi T, Antoranz Contera S, Ryan JF, et al. 2009. Dynamics of bacteriorhodopsin 2D crystal observed by high-speed atomic force microscopy. *J. Struct. Biol.* 167:153–58

114. Yan Y, Wu Y, Zou Q, Su C. 2008. An integrated approach to piezoactuator positioning in high-speed atomic force microscope imaging. *Rev. Sci. Instrum.* 79:073704

115. Yasuda R, Noji H, Kinosita K Jr, Yoshida M. 1998. F_1-ATPase is a highly efficient molecular motor that rotates with discrete 120° steps. *Cell* 93:1117–24

116. Yildiz A, Forkey JN, McKinney SA, Ha T, Goldman YE, et al. 2003. Myosin V walks hand-over-hand: single fluorophore imaging with 1.5-nm localization. *Science* 300:2061–65

117. Ying L, Bruckbauer A, Zhou D, Gorelik J, Shevchuk A, et al. 2005. The scanned nanopipette: a new tool for high resolution bioimaging and controlled deposition of biomolecules. *Phys. Chem. Chem. Phys.* 7:2859–66

118. Yokokawa M, Takeyasu K. 2011. Motion of the Ca^{2+}-pump captured. *FEBS J.* 278:3025–31

119. Yokokawa M, Wada C, Ando T, Sakai N, Yagi A, et al. 2006. Fast-scanning atomic force microscopy reveals the ATP/ADP-dependent conformational changes of GroEL. *EMBO J.* 25:4567–76

120. Zhong Q, Inniss D, Kjoller K, Elings VB. 1993. Fractured polymer/silica fiber surface studied by tapping mode atomic force microscopy. *Surf. Sci.* 290:L688–92

$\underset{R}{A}$

Contents

Index

Errata

An online log of corrections to *Annual Review of Biophysics* articles may be found at
http://biophys.annualreviews.org/errata.shtml

New From Annual Reviews:

Annual Review of Statistics and Its Application

Volume 1 • Online January 2014 • http://statistics.annualreviews.org

Editor: **Stephen E. Fienberg,** *Carnegie Mellon University*

Associate Editors: **Nancy Reid,** *University of Toronto*

Stephen M. Stigler, *University of Chicago*

The *Annual Review of Statistics and Its Application* aims to inform statisticians and quantitative methodologists, as well as all scientists and users of statistics about major methodological advances and the computational tools that allow for their implementation. It will include developments in the field of statistics, including theoretical statistical underpinnings of new methodology, as well as developments in specific application domains such as biostatistics and bioinformatics, economics, machine learning, psychology, sociology, and aspects of the physical sciences.

Complimentary online access to the first volume will be available until January 2015.

Access this and all other Annual Reviews journals via your institution at **www.annualreviews.org**.